Solid State Ionics 180 (2009) 1362–1371

Contents lists available at ScienceDirect

Solid State Ionics

journal homepage: www.elsevier.com/locate/ssi

Li mobility in $Li_{0.5-x}Na_xLa_{0.5}TiO_3$ perovskites ($0 \le x \le 0.5$) Influence of structural and compositional parameters

R. Jimenez [a], A. Rivera [b], A. Varez [c], J. Sanz [a,*]

[a] Instituto Ciencia de Materiales de Madrid, CSIC, 28049 Cantoblanco, Spain
[b] Dpto. Física Aplicada III, Universidad Complutense de Madrid, 28040 Madrid, Spain
[c] Dpto. Ciencia de Materiales, Universidad Carlos III de Madrid, 28911 Leganés, Spain

ARTICLE INFO

Article history:
Received 23 January 2009
Received in revised form 29 July 2009
Accepted 3 August 2009

Keywords:
Lanthanum lithium titanate
High temperature neutron diffraction
Perovskite structure
^{7}Li NMR spectroscopy
Ionic conductivity

ABSTRACT

The dependence of Li mobility on structure and composition of $Li_{0.5-x}Na_xLa_{0.5}TiO_3$ perovskites ($0 \le x \le 0.5$) has been investigated by means of neutron diffraction, nuclear magnetic resonance and impedance spectroscopy. At 300 K, all samples display a rhombohedral superstructure (R-3c S.G.), where octahedra are out of phase tilted along [111] direction of the ideal cubic cell. The elimination of the octahedral tilting is responsible for the rhombohedral–cubic transformation, detected near 1000 K. In these perovskites, La and Na cations are randomly distributed in A sites, but Li ions are fourfold coordinated at unit cell faces of the cubic perovskite. Lithium conductivity, $\sigma_{300\ K}$, decreases with the sodium content, decreasing from values typical of fast ionic conductors, 10^{-3} S/cm, to those of good insulators, 10^{-10} S/cm, when the interconnectivity between vacant A sites is lost ($x > 0.3$). In samples with $x < 0.3$, dc conductivity displays a non-Arrhenius behaviour, decreasing activation energy from ~0.37 to 0.25 eV when the sample is heated between 77 and 500 K. The temperature dependence of B_{Li} factors shows the existence of two regimes for Li motion. Below 373 K, Li ions remain partially located near square oxygen windows that connect contiguous A sites, but above 400 K, extended Li motions become dominant. The additional decrease of activation energy from 0.25 to 0.16 eV (low-temperature ^{7}Li NMR value), should require the full elimination of octahedral tilting which is only produced above 1000 °C.

1. Introduction

Interest in $Li_{3y}La_{2/3-y}TiO_3$ (LLTO) perovskites ($0 < y < 0.167$) has increased since the discovery of its high ionic conductivity ($10^{-3}\ \Omega^{-1}\ cm^{-1}$ at $T = 300$ K) and its possible application as solid electrolytes in batteries, sensors and other electrochemical devices [1,2]. In cubic ABO_3 perovskites, the structure is formed by a three-dimensional framework of corner-sharing BO_6 octahedra, where A cations are coordinated to 12 oxygen atoms. If the radius of A cations decreases their coordination produces the tilting of BO_6 octahedra. In $Li_{3y}La_{2/3-y}TiO_3$ series, the number of nominal vacant A sites per formula unit is $1/3 - 2y$. In Li-poor orthorhombic perovskites, $y < 0.06$, the ordering of vacancies favours a two-dimensional mobility of lithium in alternating planes [3–6]. In cubic Li-rich samples, $y > 0.1$, quenched from high temperature, the vacancy ordering is removed and Li mobility displays a three-dimensional character [6–9].

In general ionic conductivity is favoured in structures containing vacant sites which are energetically equivalent to sites occupied by mobile ions. In $Li_{0.5}La_{0.5}TiO_3$ perovskite, the absence of nominal vacancies should reduce considerably lithium conductivity; however, conductivity values are near the maximum reported in LLTO series [6]. In agreement with experimental results, Fourier map differences showed that Li ions are shifted from A positions to unit cell faces (fourfold coordinated sites) of the cubic-related perovskite [10], increasing the amount of vacant A sites which participate in conduction processes. According to this fact, the actual number of cation vacancies per formula unit, $Li_{3y}La_{2/3-y}TiO_3$, is given by the expression $n_{VT} = n_{nvac} + n_{Li} = 1/3 + y$ [11,12]. The amount of vacancies decreases with the Na content in $Li_{0.5-x}Na_x\ La_{0.5}TiO_3$ samples, decreasing ion conductivity six orders of magnitude when vacancies approach the percolation threshold of a three-dimensional network, $n_p \sim 0.31$. In the sodium end member, $Na_{0.5}La_{0.5}TiO_3$, ionic conductivity remains below 10^{-10} S/cm [11,12].

Important differences observed in two end members of the series $Li_{0.5-x}Na_xLa_{0.5}TiO_3$ ($0 \le x \le 0.5$) have motivated a deeper investigation of structure and transport properties of these compounds. The study has been carried out with neutron diffraction (ND), nuclear magnetic resonance (NMR) and impedance spectroscopy (IS) techniques. In particular, the Rietveld analysis of ND patterns, recorded at increasing temperatures, has been used to determine structural features which are responsible for percolative and non-Arrhenius

* Corresponding author. Tel.: +3491 3349075; fax: +3491 3720623.
E-mail address: jsanz@icmm.csic.es (J. Sanz).

0167-2738/$ – see front matter © 2009 Elsevier B.V. All rights reserved.
doi:10.1016/j.ssi.2009.08.002

behaviours of conductivity. In this work, the influence of the vacancy content will be first analyzed; then, the influence of the octahedral tilting on the conductivity will be investigated.

2. Experimental

2.1. Samples

Polycrystalline samples of the series $Li_{0.5-x}Na_xLa_{0.5}TiO_3$ ($0 \le x \le 0.5$) were synthesized from stoichiometric amounts of Li_2CO_3 (Aldrich 99.9%), Na_2CO_3 (Aldrich 99.9%), La_2O_3 (Aldrich 99.99%) and TiO_2 (Aldrich 99%) by solid state reaction, following the procedure described in previous work [6,12]. Li_2CO_3 and Na_2CO_3 were first dried at 600 K, La_2O_3 at 1100 K and TiO_2 at 900 K. The mixtures were then ground and heated in air up to 1600 K (1 K/min). Calcined powders were finally pressed into pellets under a pressure of 200 MPa, heated 4 h at 1600 K and quenched in air at 300 K. In high temperature treatments, a thin foil of Pt was used to avoid the reaction with alumina crucibles.

2.2. Experimental techniques

ND patterns of samples were collected between 5 and 400 K in the D2B ($\lambda = 1.594$ Å) and between 300 and 1073 K in the D1A ($\lambda = 1.913$ Å) high resolution diffractometers of the Institut Laüe-Langevin (ILL) at Grenoble. To reduce the absorption cross-section of samples, ^{7}Li enriched perovskites were prepared. ND patterns of powder samples (4 g) contained in vanadium cans were collected between 5 and 160° 2θ with a scan step of 0.02° (4 h). In Rietveld analyses, a pseudo-Voigt function was chosen to describe the lineshape of diffraction peaks (FullProf program) [13]. The coherent scattering lengths used for La, Li, Na, Ti and O atoms were respectively 8.24, −1.90, 3.63, −3.30 and 5.80 fm. In a first stage, scale factors, background coefficients, 2θ zero positions, width and peak-shape parameters were determined. In a second stage, positional parameters, site occupations and thermal factors of atoms were deduced. Anisotropic thermal factors were considered for oxygen, but isotropic ones for Ti, La, Li and Na ions.

^{7}Li and ^{23}Na NMR spectra were recorded at room temperature, after irradiation of samples with a single pulse (3 µs), in a MSL-400 Bruker spectrometer working respectively at 155.45 MHz and 104.8 MHz (external magnetic field, 9.4 T). In MAS experiments, the rotor was of Andrew type and the spinning frequency used 4 or 10 kHz. The number of scans was 100 and 400 for ^{7}Li and ^{23}Na NMR signals. The analysis of NMR spectra was carried out with the Winfit (Bruker) software package [14]. This program allows the position, linewidth, and intensity of components to be determined; however, quadrupole constants C_Q and η must be deduced by trial and error procedures. ^{7}Li spin–lattice relaxation times (T_1) were measured with the $\pi - \tau - \frac{\pi}{2}$ sequence at 30 MHz in a SXP 4/100 spectrometer. At all temperatures analyzed, the recovery of magnetization was exponential. Reciprocal spin–spin relaxation times (T_2^{-1}) were calculated from the full-width at half-maximum (FWHM) of NMR components recorded in static conditions. In the case of Gaussian lines, T_2^{-1} was calculated as 0.6π times the FWHM, in the case of Lorentzian lines, $T_2^{-1}$was calculated as π times the FWHM.

For electrical characterization, Pt/Au electrodes were deposited by d.c. sputtering onto the polished surfaces of sintered pellets (13 mm in diameter and 0.7 mm thick). In all cases, the pellets density was higher than 90% of theoretical values and the surface roughness was kept below 5 µm. For the temperature range 77–370 K, a Cryostat Janis VPF 700 coupled to a temperature controller Lakeshore 331 was used. For higher temperatures (300–500 K), one in-house jig was used. Impedance measurements were performed using an automatically controlled HP4284A precision LCR meter, working at 56 frequencies uniformly distributed between 20 Hz and 1 MHz. High and low-temperature measurements were performed under a closed air atmosphere (in-house jig) or vacuum (Cryostat), after 15 min of temperature stabilization. Non-linear least-square fittings of impedance data were performed with the EQUIVCRT program [15]. From measured impedance values (Z^*), admittance (Y^*) and relative permittivity (K^*) were calculated using the immittance relationships ($M^* = 1/K^* = j\omega C_0 Z^* = j\omega C_0 Y^*$).

3. Results

3.1. Structural analysis

ND patterns of $Li_{0.5-x}Na_xLa_{0.5}TiO_3$ quenched samples were described with the rhombohedral symmetry. In structural analyses, a hexagonal $\sqrt{2}a_p, \sqrt{2}a_p, 2\sqrt{3}a_p$ unit cell was adopted (hexagonal setting of R-3c S.G.), derived from the primitive cubic cell with parameter a_p. In this analysis, the tetragonal $a_p, a_p, 2a_p$ unit cell (P4/mmm S.G.) used previously for slowly cooled samples does not reproduce experimental profiles [16]. In Li-rich samples, a small amount of Li_2TiO_3, with main peaks at 46.7° and 98.7° 2θ, was also detected (indicated by arrows in Fig. 1 of the Supplementary material), this phase disappearing when

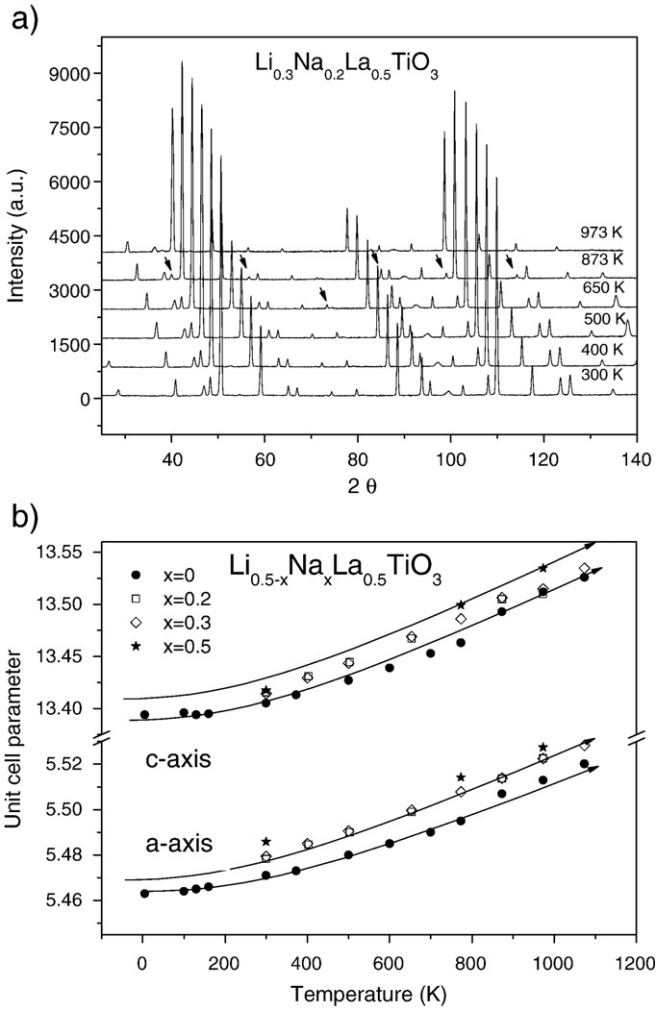

Fig. 1. (a) ND patterns of the $Li_{0.3}Na_{0.2}La_{0.5}TiO_3$ perovskite heated between 300 and 973 K. Superstructure peaks of the rhombohedral phase are indicated with arrows. ND patterns are shifted by constant amounts along x and y axes. (b) Temperature dependence of unit cell parameters of samples $x = 0$, 0.2, 0.3 and 0.5. Solid lines are given as a guide for the eye.

the Na content was increased above $x = 0.3$. The amount of this phase, estimated with the FullProf program, was always lower than 3.5%.

In all samples, unit cell parameters are near $a = 5.48$ Å and $c = 13.42$ Å. The Rietveld analysis of ND patterns, carried out with the R-3c model of Table 1, showed the presence of an out-of-phase tilting of octahedra ($5° \leq \varphi \leq 6°$) along the [111] direction of the primitive cubic cell ($a^-a^-a^-$ scheme of Glazer notation). In analyzed samples, Na and La ions are 12-fold coordinated at 6a sites, but Li ions are fourfold coordinated at 18d sites of the hexagonal unit cell. These positions correspond to the geometrical center of the cube and the faces of the cubic perovskite [10,12]. The progressive substitution of Li by Na ions reduces the amount of vacant A sites, preserving unit cell parameters (Tables 1a–d, Supplementary material). Agreement factors R_F were always lower than 4% and R_{WP} lower than 9%.

Fig. 1a shows, as an example, the temperature dependence of ND patterns of the perovskite $Li_{0.3}Na_{0.2}La_{0.5}TiO_3$. The hexagonal superstructure peaks decrease in intensity and disappear near 1000 K (arrows of Fig. 1a). At this temperature, a cubic unit cell with lattice parameter a_p (S.G.: Pm3m) was detected (see Table 1). All analyzed compositions display the same transformation that shifts towards lower temperatures as the sodium content increases. Fig. 1b shows the temperature dependence of lattice parameters in analyzed samples. In all cases, unit cell a and c parameters display similar variations.

The Rietveld analysis of ND patterns, recorded at increasing temperatures, showed similar transformations in all samples (Fig. 2). The temperature dependence of the tilting angle (φ) is given in Fig. 3a. In Na members of the series, the tilt angle decreases progressively between 300 and 1000 K; however, in the Li end member, the elimination of octahedral tilting is produced more abruptly between 800 and 1100 K. The windows between contiguous A sites, framed by four oxygen atoms, change their shape in a similar manner, as illustrated by the temperature dependence of diagonal distances, d (O–O), across these windows (Fig. 3b).

3.2. NMR spectroscopy

^{7}Li and ^{23}Na NMR spectra ($I = 3/2$) are formed by a central ($-1/2$, $1/2$) and two satellite ($1/2$, $3/2$) and ($-1/2$, $-3/2$) transitions. In spectra of static samples, the broadening of central components is mainly due to dipolar Li–Li and Li–Na interactions. In MAS-NMR experiments, central components are considerably narrowed and NMR profiles are modulated by equally spaced bands associated with the rotation of samples [12]. From spinning sideband patterns associated with satellite transitions, quadrupole C_Q and η parameters were deduced (see Table 2).

^{7}Li MAS-NMR spectra of $Li_{0.5-x}Na_xLa_{0.5}TiO_3$ samples with $x = 0$, 0.2, 0.3 and 0.4, recorded at room temperature, are given in Fig. 4a. The ^{7}Li NMR spectrum of the Li-rich end member ($x = 0$) displays a narrow signal, indicative of the high mobility of lithium ($Li^{(1)}$ species). As the Na content increases, part of lithium displays a lower mobility (increment of C_Q values of $Li^{(2)}$ species). The ^{7}Li MAS-NMR spectrum of $x = 0.3$ sample is formed by two species, which have been ascribed to mobile ($C_Q = 0$ kHz, $\eta = 0$) and fixed Li ions ($C_Q = 60$ kHz, $\eta = 0.5$) [12]. The intensity of sidebands increases at the expense of the central one when the Na content increases. Above $x = 0.3$, only fixed species were observed. Relative intensities of two components, deduced by deconvolution of ^{7}Li MAS-NMR spectra, are given as a function of the Na content in Table 2.

Table 1
Structural models used for refinement of rhombohedral[10] and cubic[9] perovskites.

S.G. R-3c[a]			S.G Pm3m		
Atom	Position	Atomic coordinates	Atom	Position	Atomic coordinates
La, Na	6a	0, 0, ¼	La, Na	1 b	½, ½, ½
Li	18 d	½, 0, 0	Li	3 *c*	½, ½, 0
Ti	6 b	0, 0, 0	Ti	1 a	0, 0, 0
O	18 e	$x \approx$ ½, 0, ¼	O	3 d	½, 0, 0

[a] Hexagonal setting.

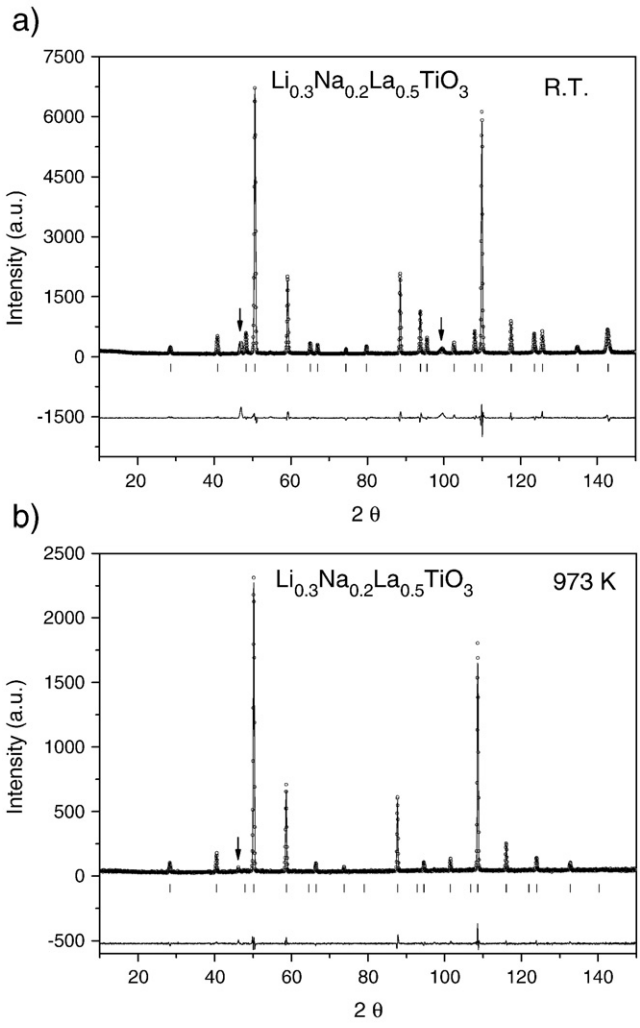

Fig. 2. Rietveld refinement of ND patterns of $Li_{0.3}Na_{0.2}La_{0.5}TiO_3$ recorded at (a) 300 and (b) 973 K. Peak positions and differences between observed and calculated profiles are also included. The arrows indicate the presence of a small amount of the Li_2TiO_3 phase.

The ^{23}Na MAS-NMR spectra of samples $x = 0.1$, 0.2, 0.3 and 0.4, recorded at room temperature, showed the presence of two components with different quadrupole constants (Fig. 4b). In samples with $x \geq 0.3$, the broad modulated component ($C_Q = 820$ kHz and $\eta = 0.5$) is preponderant, indicating that an important amount of sodium ions is fixed at distorted A sites of the perovskite ($Na^{(2)}$ species). In samples with $x < 0.3$, ^{23}Na MAS-NMR spectra are mainly formed by one intense narrow component ($C_Q = 0$ kHz and $\eta = 0$), which was tentatively assigned to mobile species ($Na^{(1)}$ species). For intermediate compositions, the intensity of the narrow component increases with the lithium content. Taking into account low conductivity values measured in $x \geq 0.3$ samples (see next section), line-narrowing effects detected in ^{23}Na NMR spectra must be ascribed to local motions of atoms (see Discussion). C_Q and η values deduced for two detected components are given in Table 2.

In order to analyze Li motions, T_2^{-1} (spin–spin) and T_1^{-1} (spin–lattice) relaxation rates, deduced from ^{7}Li NMR spectra of $x = 0$ and 0.2, samples, recorded in static conditions, are plotted *vs.* reciprocal temperature in Fig. 5. In this analysis, samples with $x \geq 0.3$, where Li mobility decreases appreciably, were not considered. In the 100–160 K range, the line shape of the central transition is Gaussian and T_2^{-1} remains constant. The line width of spectra increased slowly with the

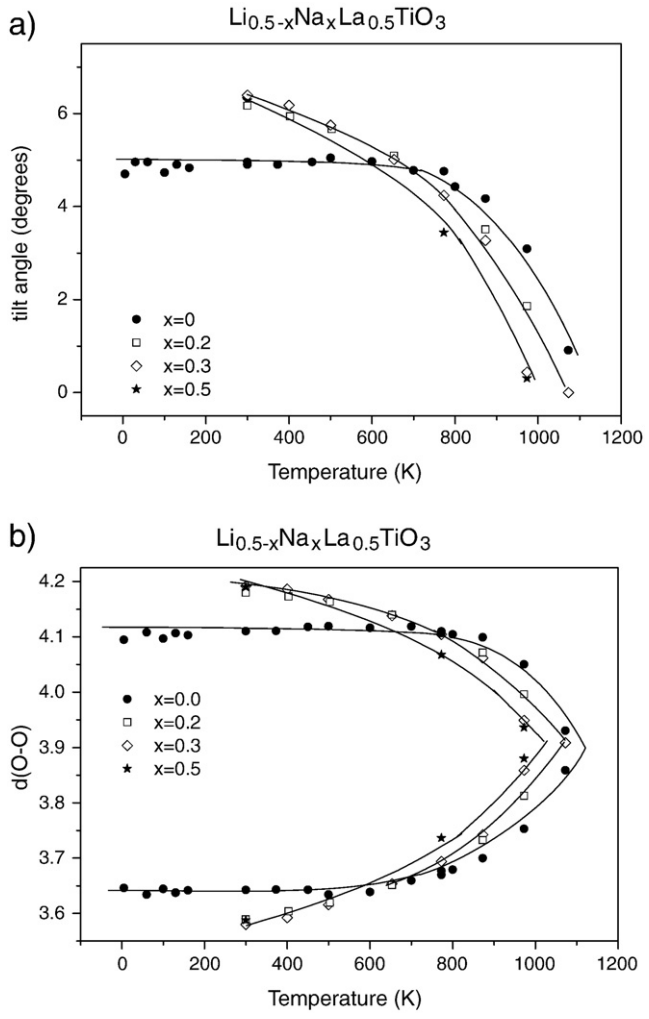

Fig. 3. (a) Tilting of TiO_6 octahedra and (b) oxygen distances across diagonals of square windows, d(O–O), that connect contiguous A sites in $Li_{0.5-x}Na_xLa_{0.5}TiO_3$ ($0 \le x \le 0.5$) perovskites.

Li content of samples (not shown). Below 125 K, nearly constant T_1^{-1} values were ascribed to relaxation induced by paramagnetic impurities. Between 125 and 160 K, local motions of lithium around equilibrium positions explain constant T_2^{-1} (dipolar Li–Li interactions) and increasing T_1^{-1} values (Li–paramagnetic interactions). Above 160 K, the line shape becomes progressively Lorentzian as a consequence of the Li motion.

When temperature increased, T_1^{-1} increases and T_2^{-1} decreased, the first reaching a maximum at 300 K. The temperature dependence of T_1^{-1} and T_2^{-1}, expressed in rad/s, can be described with equations [17,18]:

$$T_1^{-1} = C\left[\frac{\tau_c}{1+(\omega\tau_c)^{1+\beta}} + \frac{4\tau_c}{1+(2\omega\tau_c)^{1+\beta}}\right] \quad (1)$$

Table 2
NMR parameters deduced from ^{7}Li and ^{23}Na MAS-NMR spectra of $Li_{0.5-x}Na_xLa_{0.6}TiO_3$ samples, recorded at room temperature.

Sample	nLi$^{(1)}$	$C_Q^{(1)}$	nLi$^{(2)}$	$C_Q^{(2)}$	nNa$^{(1)}$	$C_Q^{(1)}$	nNa$^{(2)}$	$C_Q^{(2)}$
$x=0$	100	0	–	–	–	–	–	–
$x=0.1$	91	0	9	60	94	0	6	700
$x=0.2$	58	0	42	60	71	0	19	820
$x=0.3$	23	0	77	60	48	0	52	860
$x=0.4$	–	–	100	62	41	0	59	820

C_Q are given in kHz and n values as percentages.

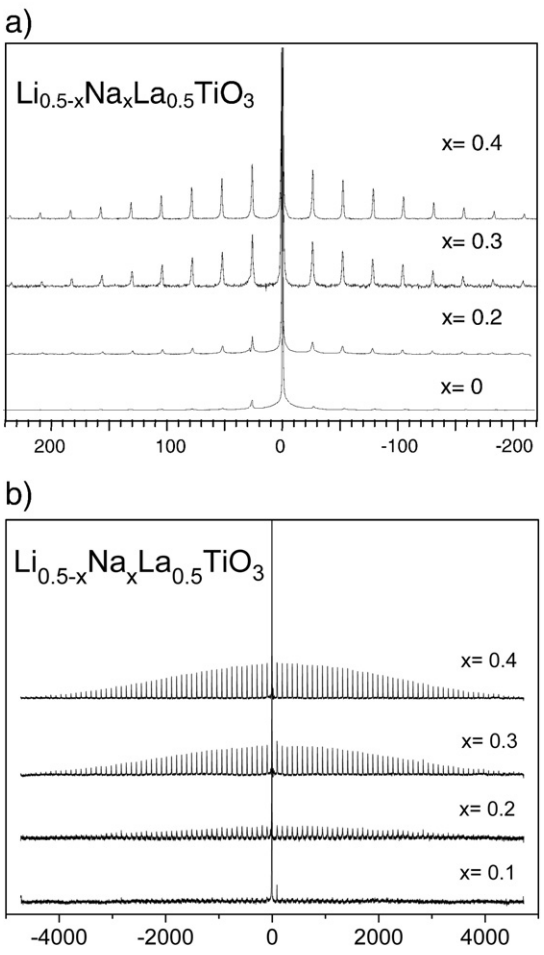

Fig. 4. (a) ^{7}Li MAS-NMR and (b) ^{23}Na-MAS-NMR spectra of $Li_{0.5-x}Na_xLa_{0.5}TiO_3$ samples recorded at room temperature. In both signals, intensity of the broad component decreases when the Li content increases.

$$T_2^{-1} = \frac{1}{2}C'\left[3\tau_c + \frac{5\tau_c}{1+(\omega\tau_c)^{1+\beta}} + \frac{2\tau_c}{1+(2\omega\tau_c)^{1+\beta}}\right] \quad (2)$$

where C and C' depend on the magnetic interactions which cause nuclear relaxation, β is a constant that takes into account correlation effects in Li motions and τ_c is the residence time at structural sites. The temperature dependence of τ_c is given by the expression

$$\tau_c = \tau_{c_0} exp\left(E_M^{NMR}/kT\right) \quad (3)$$

where k is the Boltzmann constant, τ_{c_0} is the residence time of atoms at infinite temperature and E_M^{NMR} is the activation energy deduced from the high temperature branch of $1/T_1$ maxima. Activation energy deduced from the low-temperature branch of the maximum, denoted E_m^{NMR}, has been often related to that deduced from the high temperature branch, E_M^{NMR}, by the expression $E_m^{NMR} = E_M^{NMR} \times \beta^{NMR}$ [18].

3.3. Electrical characterization

The frequency dependence of conductivity, measured at 230 K in $x=0$, 0.1, 0.2 and 0.3 samples, is given in Fig. 6a. A dc plateau, ascribed to the "bulk" response, was observed in samples with high Li content ($x \le 0.2$), which shifted to lower frequencies when the Na content increases. In these samples, a fast decay of conductivity was observed at low frequencies, indicating the presence of interfacial grain-boundary blocking processes. In samples with $x > 0.2$, the "bulk"

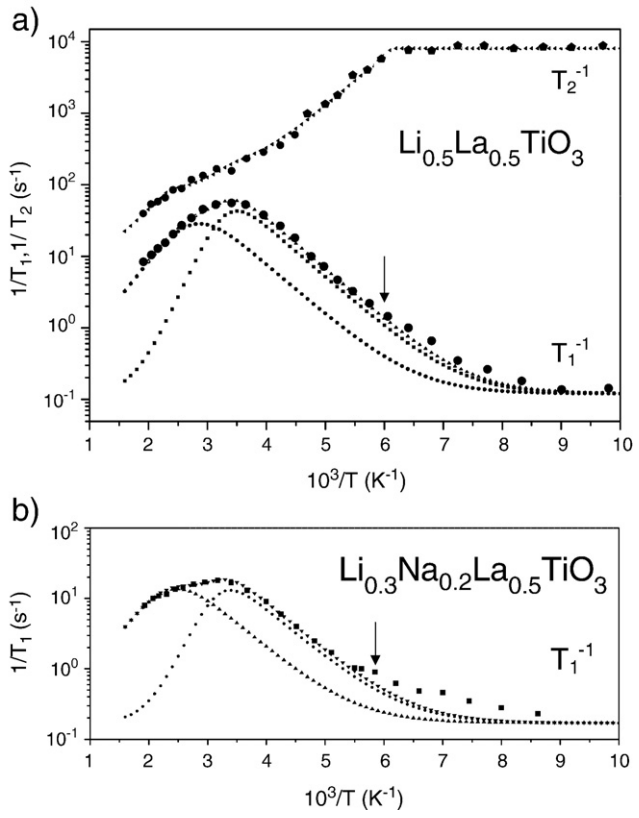

Fig. 5. Temperature dependence of ^{7}Li NMR spin–lattice ($1/T_1$) and spin–spin ($1/T_2$) relaxation rates measured at 30 MHz in (a) $Li_{0.5}La_{0.5}TiO_3$ ($x=0$) and (b) $Li_{0.3}Na_{0.2}La_{0.5}TiO_3$ ($x=0.2$) samples. Arrows indicate temperatures above which Li hops to contiguous A cavities. Experimental values were fitted to two relaxation mechanisms described with modified BPP expressions (see text).

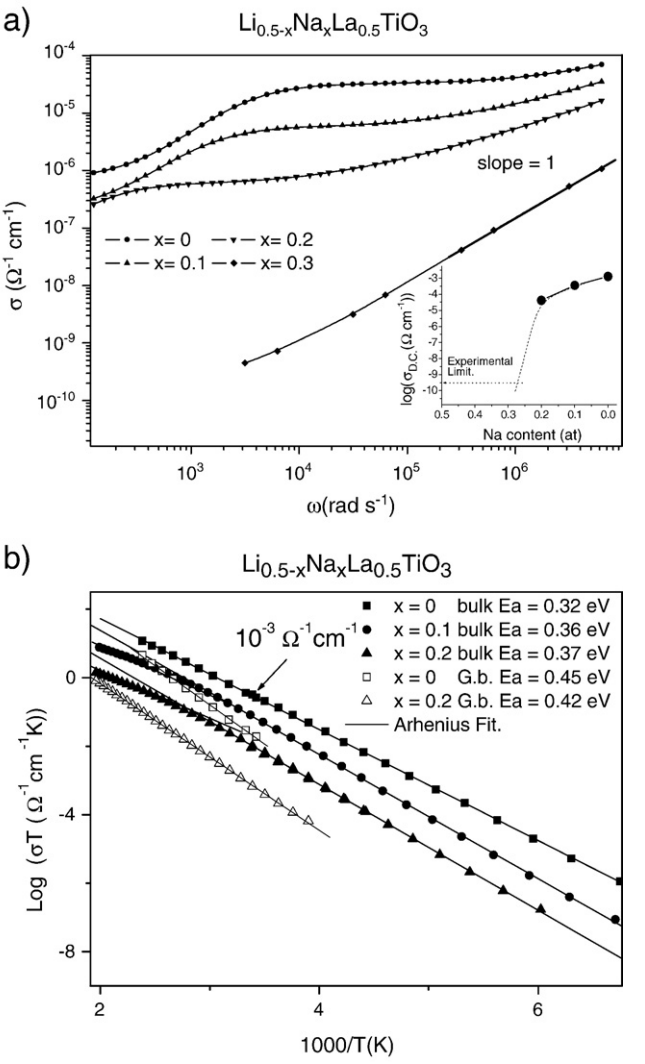

Fig. 6. (a) Frequency dependence of conductivity of $Li_{0.5-x}Na_x\ La_{0.5}TiO_3$ samples ($x=0$, 0.1, 0.2 and 0.3) measured at 230 K. In the inset, the compositional dependence of dc conductivity, measured at 300 K, is given. (b) Temperature dependence of bulk (closed symbols) and grain-boundary (open symbols) conductivities of samples $x=0$, 0.1, and 0.2.

plateau was not detected. The change of slope detected below 10^4 rad s^{-1} in the conductivity plot of $x=0.3$ sample, corresponds to the crossover between the constant loss regime (slope near to 1) and the universal dielectric response ascribed to Li motions [19].

The equivalent circuit used in the analysis of electrical impedance results is formed by the series association of two impedance relaxations, used to describe bulk and grain-boundary contributions. From the analysis of low-temperature results, the electrical response of the bulk contribution was first deduced. In subsequent stages, grain boundary and electrode blocking responses were determined. In this analysis, conductivity values were fitted to the expression

$$\sigma^* = \left[1/\sigma_1{}^* + 1/(\sigma_2{}^* + A\cdot\omega^p)\right]^{-1} \quad (4)$$

where asterisks denote complex conductivity, and $\sigma_1{}^*$ and $\sigma_2{}^*$ account for grain boundary and bulk conductivities. $\sigma_1{}^*$ and $\sigma_2{}^*$ were assumed to adopt the form $\sigma_{dc}+B(i\omega)^n$, where n has been suggested to describe correlation effects in Li^+ motions [20]. In this expression, the term $A\omega^p$ was included to take into account the near constant loss regime ($p\sim1$) detected at low temperature [19] (Fig. 6a). In Fig. 2 of the Supplementary material, an example of the fitting of complex impedance data to the proposed model is given.

From the frequency dependence of bulk conductivity values, the dispersion parameter n, deduced from the low-temperature region (160–300 K) was determined. In all cases, n values are near 0.64 ± 0.02 (Table 3). The inset of Fig. 6a shows the compositional dependence of dc conductivity of $Li_{0.5-x}\ Na_xLa_{0.5}TiO_3$ samples, measured at 300 K (filled in circles). Samples with low sodium content ($x<0.2$) display dc-conductivity values near 10^{-3} S/cm at 300 K. The striking result is the sharp decrease observed on conductivity near $x\sim0.2$. When sodium content increases, $x\geq0.3$, dc conductivity is found to be lower than 10^{-10} S/cm, our experimental limit.

The temperature dependence of bulk (close symbols) and grain-boundary (open symbols) conductivities is analyzed in Fig. 6b. Activation energies deduced from the low-temperature region of bulk conductivity ($T<300$ K) increased from 0.32 to 0.37 eV, when the amount of Na increased from 0 to 0.2. These results agree with those deduced from the temperature dependence of the crossover ω_p frequency, located between the low frequency dc plateau and the power-law ac- regime of conductivity (Fig. 7a). Activation energies, deduced for the grain-boundary conductivity of $x=0$ and 0.2 samples, were respectively 0.45 and 0.42 eV. In analyzed samples, bulk and grain-boundary conductivities tend to converge at increasing temperatures. For the Li end member of the series, activation energies decrease from 0.32 to 0.29 eV between 250 and 500 K. For Na containing samples, the activation energy decreases from 0.36 to 0.24 eV in the same temperature range. Low resistance values measured for Pt/Au electrodes, 0.46 Ω at 300 K and 0.63 Ω at 525 K, do not affect the bending observed in dc-conductivity plots.

The temperature dependence of the relative permittivity K' is shown in Fig. 7b. Two different behaviours were observed in analyzed samples. In Li-rich samples ($x\leq0.2$), K' values increase monotonically

Table 3
Parameters deduced from the fitting of ^{7}Li NMR T_1^{-1} and T_2^{-1}relaxation data, measured between 100 and 500 K in $Li_{0.5}La_{0.5}TiO_3$ ($x=0$) and $Li_{0.3}Na_{0.2}La_{0.6}TiO_3$ ($x=0.2$) samples.

Sample	$\beta=1-n$[a]	Ea (L.T)[a] (eV)	C (s^{-2})[a]	τ_0[a] (s)	$\beta=1-n$[b]	Ea (H.T)[b] (eV)	C (s^{-2})[b]	τ_0[b] (s)
$x=0.0$	0.39 ± 0.02	0.34 ± 0.02	$5.5\cdot10^9$	$1\cdot10^{-14}$	0.50 ± 0.04	0.28 ± 0.03	$3.4\cdot10^9$	$1\cdot10^{-14}$
$x=0.2$	0.40 ± 0.02	0.35 ± 0.02	$1.5\cdot10^9$	$7.5\cdot10^{-15}$	0.65 ± 0.04	0.22 ± 0.03	$1.7\cdot10^9$	$8\cdot10^{-12}$

[a] L.T: temperature range 160–300 K.
[b] H.T: temperature range 300–500 K.

with temperature, reaching successive plateaus when Li mobility is restricted inside A cavities (K' values near 10^2), or blocked at internal interfaces (K' values near 10^3), grain-boundaries (K' values near 10^5) and electrolyte-electrode interfaces (K' values $\geq 10^6$) [21]. In samples with a higher Na content, $x>0.2$, the absence of ionic dc conductivity produces a flat dielectric response. In this case, a broad small maximum was detected at ~165 K that shifts to lower temperatures when the measuring frequency decreases. The activation energy deduced from the associated loss peak is 0.37 eV. This peak shifts to lower temperatures when the Na content increases. For $x\geq0.4$, the maximum in K' is shifted out of the experimental window.

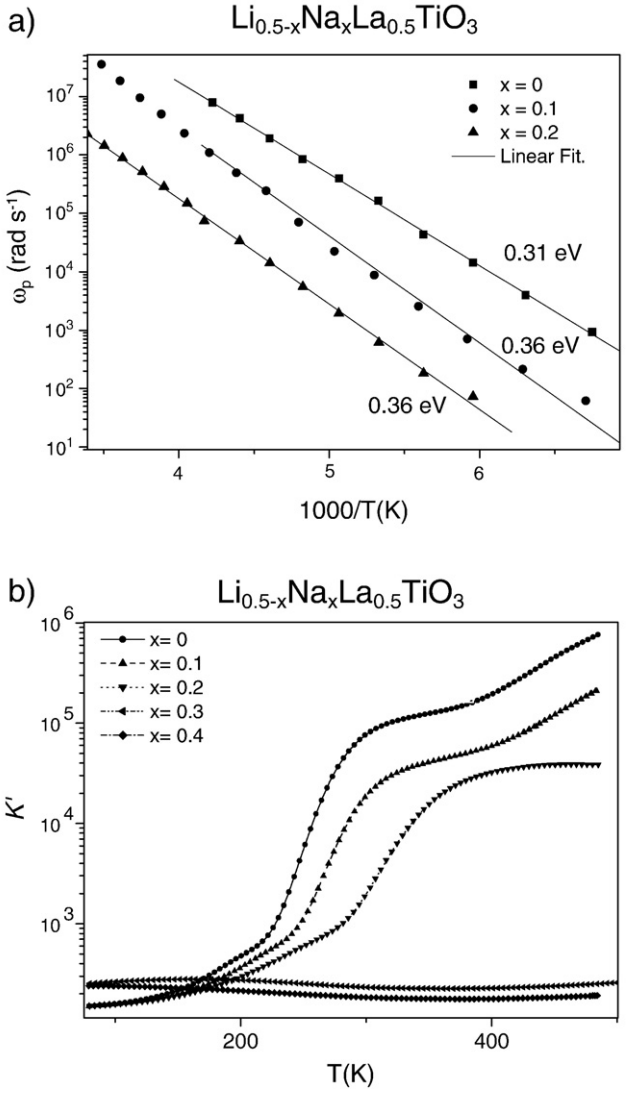

Fig. 7. (a) Temperature dependence of the crossover ω_p frequency in samples $x=0$, 0.1 and 0.2. (b) Temperature dependence of the relative permittivity K' of $x=0$, 0.1, 0.2, 0.3 and 0.4 samples, measured at 100 Hz. In this figure, the electrical behaviour of samples changes considerably at both sides of the percolation threshold.

4. Discussion

All $Li_{0.5-x}Na_xLa_{0.5}TiO_3$ ($0\leq x\leq0.5$) samples display at room temperature a rhombohedral (R-3c S.G.) symmetry. Unit cell parameters do not change appreciably with composition, indicating that the substitution of Li by Na does not affect the perovskite framework. In analyzed perovskites, Na ions occupy the centre of 12 coordinated A-polyhedra, but smaller Li cations are fourfold coordinated at unit cell faces of the primitive cubic cell. The heating of $Li_{0.5-x}Na_x$ $La_{0.5}TiO_3$ perovskites produces near 1000 K the elimination of the octahedral tilting, responsible for the rhombohedral distortion of samples. Above 1100 K, all samples display the cubic (Pm-3m S.G.) symmetry.

4.1. Li mobility

In Li-rich members of $Li_{0.5-x}Na_xLa_{0.5}TiO_3$ perovskites ($x\leq0.2$), ion conductivity displays one of the highest values reported in the literature (~10^{-3} Ω^{-1} cm^{-1} at $T=300$ K) (inset of Fig. 6a). In order to explain Li motion mechanisms, NMR and electrical impedance results have been analyzed between 100 and 500 K. In this study, samples below the percolation threshold ($x>0.3$), with two different populations of Li, have not been considered. In these samples, conductivity values are low and the analysis of relaxation effects becomes difficult.

4.2. NMR spectroscopy

Li mobility decreases the linewidth of central NMR components ($1/T_2$) and increases T_1^{-1} values (see Fig. 5a). At the T_1^{-1} maximum, ($\omega_0\tau_c=1$), the residence time of Li ions at occupied sites is $\tau_c\approx\omega_0^{-1}\approx 5\cdot10^{-9}$ s.

In the $Li_{0.5}La_{0.5}TiO_3$ sample, the analysis of T_1 and T_2 relaxation times, measured at 30 MHz in the temperature range 100–500 K, showed the existence of several stages for Li mobility. At low temperatures, Li motion is restricted inside large A cavities of the perovskite, producing the constant loss regime detected at low temperatures in conductivity measurements [19]. In this regime, T_1^{-1} values increase but T_2^{-1}remains almost constant, indicating that dipolar Li–Li interactions do not change appreciably between 120 and 160 K [19]. Above this temperature range, Li^+ ions hop to contiguous cavities, passing through oxygen square windows (new regime detected above 160 K in T_1^{-1} plots); however, Li motions display a high degree of correlation, making still probable reverse hopping processes [22]. In this regime, the diffusion coefficient, measured at 300 K with the pulse field gradient NMR technique, was ~$1.2\cdot10^{-12}$ m^2/s. This value agrees with that calculated by the Einstein expression

$$D = l^2 / (6\tau_{CM}) \quad (5)$$

when the residence time of Li ions at structural sites ($\tau_{CM}\sim5\times10^{-9}$ s) deduced from $1/T_1$ maxima, and the distance between equivalent sites ($l\sim3.9$ Å) are considered.

However, the T_1^{-1} maximum is broader than expected for a single BPP mechanism. In order to reproduce the temperature dependence of T_1^{-1} and T_2^{-1}values, we have considered the expressions

$$\frac{1}{T_1} = \frac{1}{T_1^{LT}} + \frac{1}{T_1^{HT}} + \frac{1}{T_1^{PAR}} \quad (6)$$

$$\frac{1}{T_2} = \frac{1}{T_2^{LT}} + \frac{1}{T_2^{HT}} + \Delta\omega \quad (7)$$

where $(T_1^{LT})^{-1}$, $(T_2^{LT})^{-1}$ and $(T_1^{HT})^{-1}$, $(T_2^{HT})^{-1}$ stand for low and high temperature mechanisms, both described with expressions (1) and (2). In the absence of lithium motion ($T<160$ K), $\Delta\omega$ increases with dipolar interactions; and T_1^{PAR} decreases with paramagnetic interactions.

In $Li_{0.5}La_{0.5}TiO_3$ ($x=0$) perovskite, the activation energy measured between 160 and 300 K was $E_m^{NMR}=0.15$ eV. In the high temperature regime, 300–500 K, the activation energy deduced for Li motion was $E_M^{NMR}=0.28$ eV (see Table 3). In the case of the sample $Li_{0.3}Na_{0.2}La_{0.5}TiO_3$ ($x=0.2$), similar results were obtained; however, the maximum decreased and shifted slightly towards higher temperatures. In analyzed samples, the two relaxation mechanisms have been ascribed to two types of motions with the same microscopic activation energy, E_m, but different degree of correlation, β (see Table 3). In two analyzed samples, E_m~0.14 eV and β~0.37, giving $E_M=E_m/\beta$~0.36 eV for the low-temperature regime [23,24]. This value coincides with that deduced from conductivity data recorded between 160 and 300 K. Above 373 K, activation energies, E_M, decrease and Li motions become less correlated [25,26]. The fitting of experimental results provided parameters included in Table 3. In general, parameters deduced are less precise in the high temperature regime where relaxation data were taken in a shorter interval.

NMR T_1^{-1} data could also be interpreted with a distribution of correlation times, which changes with temperature. However, the dependence of electrical modulus on frequency should also change with temperature in this case, which has not been observed [26]. β values were also estimated in a previous work from the analysis of the frequency dependence of T_1^{-1} values, measured at 10, 20 and 30 MHz, in the low-temperature regime of T_1^{-1} maxima [27]. This analysis gave again a β value ~0.4 at 300 K, when using the expression $T_1^{-1}(\omega_0)::\omega_0^{-(1+\beta)}$. These results confirm the validity of hypotheses assumed in coupling and jump relaxation models [23,24], but do not support the alternative model based on distributions of correlation times.

4.3. Electrical characterization

In $Li_{0.5-x}Na_xLa_{0.5}TiO_3$ samples, changes observed on relative permittivity K' have been related to successive interfacial blockings of lithium, which increase progressively the dielectric permittivity of samples [21] (Maxwell–Wagner processes). This effect is clearly observed in the $x=0$ sample, where Li^+ blockings at grain boundary and electrode surfaces have been ascribed to two plateaus detected at 300 and 500 K. These processes were shifted to higher temperatures in Na-bearing samples as a consequence of their lower conductivity ($x=0.1$ and 0.2). In $x=0.3$ and 0.4 samples, no successive plateaus were detected, indicating that only local Li motions are produced inside particles (absence of long range motions). For low Li contents, $x>0.3$, K' values measured at low temperature are higher than those measured in samples with higher Li contents. In this case, the existence of a broad maximum in K' plots is indicative of the polar behaviour produced by the localization of Li^+ and Na^+ ions in perovskites. Similar conclusions were deduced from the analysis of ^7Li and ^{23}Na MAS-NMR spectra recorded at room temperature.

From the analysis of the frequency dependence of conductivity, σ_{dc} values, n exponents and crossover frequencies $\omega_p=(B\cos(n\pi/2)/\sigma_{dc})^{(-1/n)}$ were deduced [20]. In the low-temperature regime, 160–300 K, n values are near 0.64 in $x=0$, 0.1 and 0.2 samples (Table 4). In general, n values vary with the network dimensionality [28]. In 3D conductors, n values are in the range 0.64–0.70. In 2D ionic conductors, like Na β-alumina and Ag β-alumina, n values are in the range 0.51–0.60. Finally, in 1D ionic conductors, like priderite or hollandite, n values are in the range 0.2–0.4. According to reported data, Li^+ ions display a 3D mobility in $Li_{0.5-x}Na_xLa_{0.5}TiO_3$ samples.

In general, dc conductivity can be expressed as

$$\sigma_{dc}\cdot T = \boldsymbol{K_n}\cdot\omega_p = \boldsymbol{K_n}\cdot\omega_e\cdot\exp(-E_M/kT) = \boldsymbol{K_n}\omega_0\cdot\exp(-E_M/kT)\cdot\exp(\Delta S_M/k). \quad (8)$$

where $\boldsymbol{K_n}\omega_e$ is the pre-exponential factor, and E_M and S_M are the activation energy and entropy associated with Li migration respectively. In this expression, ω_e stands for the crossover ω_p frequency extrapolated to infinite temperature, ω_0 is the attempt frequency and $\boldsymbol{K_n}$ is a factor proportional to the charge carrier concentration.

In the range 160–300 K, bulk conductivity decreases and activation energy increases with the Na content from 0.32 to 0.37 eV (Fig. 6b and Table 4). In agreement with previous work, the macroscopic activation energy, E_M, was related to the microscopic energy, E_m, through the expression $E_m=E_M\cdot(1-n)$ [23,24]. In the case of $x=0.1$ sample, $E_M=0.36$ eV and $n=0.63$, which gives $E_m=0.14$ eV. This value is close to the activation energy deduced from the low-temperature branch of the NMR T_1^{-1} maximum.

In order to further analyze Li motions, pre-exponential $\boldsymbol{K_n}\omega_e$ factors, deduced from the extrapolation of dc-conductivity values to infinite temperatures, have been analyzed in $x=0$, 0.1 and 0.2 samples (see Table 4). $\boldsymbol{K_n}\omega_e$ factors decrease from 85113 ($x=0$ sample) to 18853 Scm^{-1} K ($x=0.2$ sample) when the Na increases. Furthermore, ω_e parameters were deduced from the extrapolation of crossover ω_p values to infinite temperature (Table 4). Samples $x=0$ and $x=0.1$ present similar ω_e values, while a drop of one order of magnitude was obtained in $x=0.2$ sample.

At this point it is important to discuss the physical meaning of ω_e deduced from expression (8). Following Nowick's ideas

$$\omega_e = \omega_0\exp(\Delta S_M/k) \quad (9)$$

ω_e can be understood as an effective frequency for Li motions [29,30]. In samples $x=0$ and 0.1, ω_e values are practically the same, so changes in Li mobility must be ascribed to those produced in activation energy. At increasing Na contents, activation energy increases slightly, but ω_e drops one order of magnitude (Table 4). In this case, changes detected on ω_e must be ascribed to those produced in the migration entropy.

Finally, the pre-exponential $\boldsymbol{K_n}$ factor can be estimated with the expression[20]

$$\boldsymbol{K_n} = z\cdot f\cdot\left(n_c q^2\right)\cdot\left(l^2/6\right)\cdot c(1-c)/k \quad (10)$$

where q is the carrier charge, n_c is the density of mobile ions (8.6×10^{21} Li/cm^{-3} in $Li_{0.5}La_{0.5}TiO_3$) and l is the distance (3.86 Å) to the z nearest-neighbour equivalent sites (z~6), having the probability c of being occupied by mobile ions and $(1-c)$ the probability of being empty (0.16 and 0.84 in $x=0$ sample). In this expression, f is the self diffusion correction factor (near unity) and k is the Boltzman constant.

In $x<0.3$ conducting samples, $\boldsymbol{K_n}\omega_e$ values calculated with the expression (10) are similar to those deduced from experimental results, indicating that most of lithium participates in diffusion processes. On the other hand, it is interesting to analyze the compositional dependence of the $\boldsymbol{K_n}$ term, deduced from $\boldsymbol{K_n}\omega_e$ and ω_e values [20]. It is observed that $\boldsymbol{K_n}$ values increase slightly with Na content in samples with $x<0.3$ (see Table 4). Taking into account that the $c(1-c)$ factor decreases with the Na content, the small increment

Table 4
Parameters deduced from a.c. and d.c. conductivity data of the bulk response, following Ref. [20].

Sample	n[a,b]	Ea (L.T)[b] (eV)	$K_n \cdot \omega e$ (Scm^{-1} K)[b]	ωe (rad s^{-1})[b]	K_n (Scm^{-1} K s^{-1})[b]	Ea (H.T)[c] (eV)
$x=0.0$	0.64 ± 0.02	0.32 ± 0.02	$85{,}113\pm300$	$3.20\pm0.2\cdot10^{13}$	$1.67\pm0.6\cdot10^{-9}$	0.30 ± 0.03
$x=0.1$	0.63 ± 0.02	0.36 ± 0.02	$115{,}835\pm600$	$4.07\pm1.0\cdot10^{13}$	$2.69\pm0.3\cdot10^{-9}$	0.23 ± 0.03
$x=0.2$	0.65 ± 0.02	0.37 ± 0.02	$18{,}853\pm50$	$3.27\pm0.5\cdot10^{12}$	$3.5\pm0.3\cdot10^{-9}$	0.24 ± 0.03

[a] A.C.: conductivity dispersion parameter.
[b] L.T: temperature range 160–300 K.
[c] H.T: temperature range 300–500 K.

detected on the K_n factor must be ascribed to changes produced in geometrical factors.

The analysis of conductivity values measured between 300 and 500 K showed a clear departure from the Arrhenius behaviour in Na-bearing samples which was not detected in the Li-rich end member of the series. Similar results were obtained in analysis of ^{7}Li NMR relaxation times (Tables 3 and 4). In the temperature range 300–500 K, activation energies E_M of samples decreased progressively, without attaining a new linear regime in conductivity plots (Fig. 6). To better analyze the high temperature regime, a larger temperature and frequency range needs to be explored in spectroscopic determinations.

4.4. Structural factors affecting Li mobility

4.4.1. Octahedral tilting

The analysis of conductivity plots suggests the existence of two regimes for Li motion. In these regimes, activation energy, E_M, deduced from conductivity data decreases from 0.36 to 0.25 eV when temperature increases from 300 to 500 K. If activation energy E_M is related to the microscopic energy, E_m, through the expression $E_M = E_m/(1-n)$, changes produced in activation energy E_M should be ascribed to those produced in the correlation factor $(1-n)$, because E_m is supposed to remain constant [23,24]. Consistent with this, n values should decrease from 0.63 to 0.44 when temperature increases from 300 to 500 K. If correlation effects were fully eliminated, $n=0$, activation energy E_M should coincide with that deduced from the low-temperature branch of T_1^{-1} NMR maximum, $E_M = E_m = 0.14$ eV [23]. This stage was attained at 500 K in $Li_{0.2-x}Na_xLa_{0.6}TiO_3$ series, but in this work higher temperatures are required to eliminate completely correlation effects in $Li_{0.5-x}Na_xLa_{0.5}TiO_3$ perovskites [30].

The departure of conductivity from the Arrhenius behaviour has been related to the existence of a saturation limit for Li conductivity, when the influence of structure decreases. In this new regime, correlation effects on Li motions are completely eliminated [31–33]. Similar observations were found in the crystalline fast ionic conductor Na β″-alumina. In this case, the bending of conductivity plots was related to order-disorder transitions in the Na sublattice, which produced the cation clustering and the increment of activation energy observed at low temperature [34,35]. This behaviour was not observed in Na β′-alumina where neither cation clustering nor phase transitions were produced [36]. In the $Li_xLa_{2/3-x}TiO_3$ series, a departure of dc conductivity from the Arrhenius behaviour has been reported [1,26,37]. In some cases, the temperature dependence of conductivity has been described with the Vogel–Tamman–Fulcher formalism; however, structural reasons responsible for this behaviour have not been discussed [37,38].

In order to better analyze structural reasons that enhance Li mobility in $Li_{0.5-x}Na_xLa_{0.5}TiO_3$ perovskites, geometrical changes produced in octahedral tilting and square windows are analyzed in Fig. 3. The elimination of octahedral tilting, associated with the rhombohedral–cubic transition, was produced between 400 and 1000 K in Na-bearing samples, but only above 800 K in the Li member, $Li_{0.5}La_{0.5}TiO_3$. According to this fact, distortions of square windows are important at low temperatures (3.60×4.15 Å), but disappear progressively when octahedral tilting is eliminated (3.9×3.9 Å). Based on these results, progressive changes detected in activation energies of Li have been ascribed to modifications produced in square windows geometry (Fig. 3b). In agreement with structural data, these changes can be observed above 400 K in Na-bearing samples ($x>0.2$); but, they require higher temperatures in the Li end member of the series.

On the other hand, the temperature dependence of atomic thermal factors is analyzed in Figs. 8 and 9. In general oxygen thermal factors, B_O, are higher than those of titanium, B_{Ti}, suggesting that some oscillation of octahedra could be produced. A deeper analysis of oxygen factors, B_O, indicated the existence of two regimes in $Li_{0.5}La_{0.5}TiO_3$ perovskite: in the temperature interval 300–700 K, the increment of B_O factors was moderate, but above 700 K the increment becomes important. In the first case, only the expansion of the unit cell was detected; in the second case, changes on the octahedral tilting

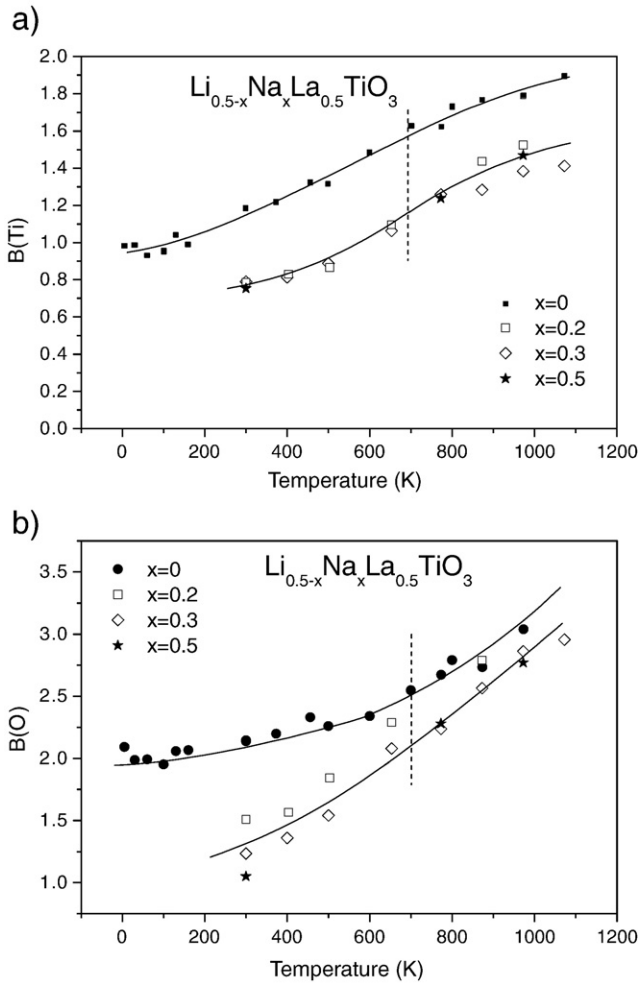

Fig. 8. Temperature dependence of isotropic thermal factors of (a) Ti and (b) O atoms in $Li_{0.5-x}Na_xLa_{0.5}TiO_3$ samples. Solid lines are given as a guide for the eye.

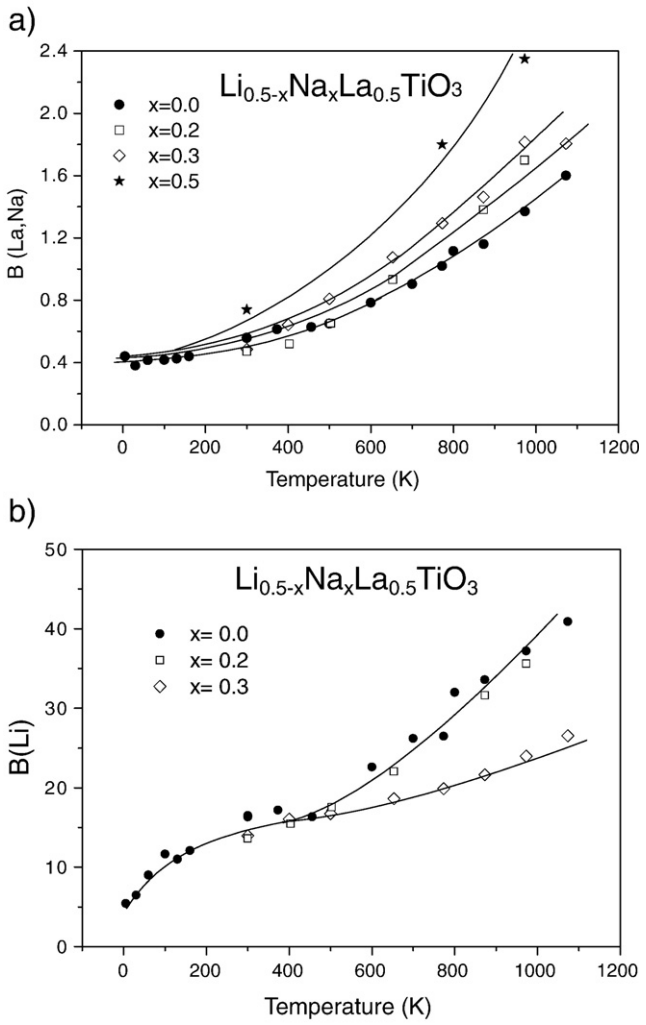

Fig. 9. Temperature dependence of isotropic thermal factors of: (a) La and (b) Li atoms in $Li_{0.5-x}Na_xLa_{0.5}TiO_3$ samples. Solid lines are given as a guide for the eye.

make possible the rhombohedral–cubic transformation (Fig. 3). Obtained results are slightly different in other members of the $Li_{0.5-x}Na_xLa_{0.5}TiO_3$ series, where the positional disorder was lower and the octahedral tilting was progressively eliminated between 400 and 1100 K.

Taking into account that coordination of Li ions with oxygen atoms is not possible at A sites, the location of lithium at the centre of unit cell faces of pseudocubic perovskites is produced [10,11]. In all analyzed samples, lithium thermal factors increase considerably when temperature increases and localization of Li is difficult to determine at 773 K (see Fig. 9b). A deeper analysis of the temperature dependence of B_{Li} values indicates that the increment in Li mobility is produced in two stages. Below 400 K, mobility of Li displays some local character; however, above 400 K, more extended motions are produced which impede the determination of the lithium position. Similar results were deduced from the analysis of T_1^{-1} plots vs. temperature, where two relaxation mechanisms with different correlation degree were detected below and above 400 K. In the case of $x = 0.3$, the absence of extended motions reduces considerably the contribution of the second regime to B_{Li} plots (see Fig. 9b). Both regimes, associated with the conductivity departure from the Arrhenius behaviour, precede the rhombohedral–cubic transformation.

Finally, thermal factors of La atoms increase with the Na content, suggesting that Na ions display higher thermal factors than La, but considerably lower than Li ions (Fig. 9a). However, taking into account that diagonal d(O–O) distances of square windows (3.9 and 4.7 Å) always remain below 2 d(O–Na) distances (5.6 Å deduced from Shannon radii [39]), diffusion of Na should not be produced. In consequence, the decrease observed on ^{23}Na NMR C_Q parameters of Li-rich samples should be ascribed to local motions of lithium that reduce considerably the contribution of Li to electric field gradients produced at Na positions. This interpretation is supported by parallel changes detected at 300 K on relaxation T_1^{-1} times of ^7Li and ^{23}Na NMR signals of $Li_{0.5-x}Na_x$ $La_{0.5}TiO_3$ perovskites [12]. In both signals, the cancellation of quadrupolar interactions is observed when Li motion is produced (Fig. 4a and b).

5. Conclusions

Structure and Li mobility have been analyzed in rhombohedral $Li_{0.5-x}Na_xLa_{0.5}TiO_3$ ($0 \le x \le 0.5$) perovskites by means of ND, NMR and impedance spectroscopy. At room temperature, ND patterns have been described with an hexagonal $\sqrt{2}a_p,\sqrt{2}a_p,2\sqrt{3}a_p$ unit cell (hexagonal setting of the R-3c S.G.), in which octahedra are tilted along the [111] direction of the primitive cubic cell ($a^-a^-a^-$ scheme in Glazer notation). The Rietveld analysis of ND patterns showed that Na and La ions occupy A sites, while Li ions are located at the center of unit cell faces of the related cubic perovskite. In all cases, the elimination of the octahedral tilting is responsible for the rhombohedral–cubic transformation. In samples heated at 1100 K, a cubic a_p,a_p,a_p unit cell (S.G. Pm-3m) was detected.

The substitution of Li^+ by Na^+ ions decreases the amount of vacancies, reducing dc conductivity of samples. However, Li conductivity decreases several orders of magnitude, from 10^{-3} to 10^{-10} S/cm, when the amount of vacancies approaches the percolation threshold of perovskites ($n_p = 0.31$). Below the percolation threshold, Li ions only display local mobility, remaining confined in small structural domains. Described results confirm the important role played by the amount of vacant A sites on Li conductivity of $Li_{0.5-x}$ $Na_xLa_{0.5}TiO_3$ perovskites.

In $Li_{0.5-x}Na_xLa_{0.5}TiO_3$ perovskites, conductivity values depart considerably from the Arrhenius behaviour. In the temperature range 200–500 K, the decrement observed in activation energy from ~0.35 to 0.25 eV has been ascribed to the partial elimination of the octahedral tilting. In Na-bearing samples, this elimination is produced at lower temperatures than in the Li end member. However, the expected decrement from 0.35 to 0.16 eV (microscopic activation energy deduced from NMR results) requires the full elimination of correlation effects, which is only produced at 1000 K, when the octahedral tilting of perovskites is completely eliminated. Successive Maxwell–Wagner blocking processes, detected in the real part of dielectric constant plots, have been ascribed to lithium blocking inside unit cells, structural domains, grain boundary and electrode interfaces.

Acknowledgments

We thank the Spanish Agency CICYT (MAT2007-64486-C07 projects) and the Regional Government of Madrid (Project S-505/PPQ-0358) for financial support. Authors thank ILL for neutron beam time allocation and Bruker Ltd Company (Germany) for NMR pulse field gradient determinations. Authors thank C. León, J. Santamaría and M.T. Fernandez for helpful discussions.

Appendix A. Supplementary data

Supplementary data associated with this article can be found, in the online version, at doi:10.1016/j.ssi.2009.08.002.

References

[1] Y. Inaguma, C. Liquan, M. Itoh, T. Nakamura, T. Uchida, H. Ikuta, M. Wakihara, Solid State Commun. 86 (1993) 689.

[2] A.G. Belous, G.N. Novitskaya, S.V. Polyanetskaya, Y. Gornikov, I. Yu, Izv. Akad. Nauk SSSR, Neorg. Mater. 23 (1987) 470.
[3] Y. Inaguma, T. Katsumata, M. Itoh, Y. Morii, J. Solid State Chem. 166 (2002) 67.
[4] A.I. Ruiz, M.L. López, M.L. Veiga, C. Pico, Solid State Ionics, 112 (1998) 291.
[5] M.A. París, J. Sanz, C. León, J. Santamaría, J. Ibarra, A. Várez, Chem. Mat. 12 (2000) 1694.
[6] J. Ibarra, A. Várez, C. León, J. Santamaría, L.M. Torres-Martínez, J. Sanz, Solid State Ionics 134 (2000) 219.
[7] H. Kawai, J. Kuwano, J. Electrochem Soc. 147 (1994) L78.
[8] A.D. Robertson, S. García-Martín, A. Coats, A.R. West, J. Mater. Chem. 5 (1995) 1405.
[9] Y. Harada, Y. Hirakoso, H. Kawai, J. Kuwano, Solid State Ionics 121 (1999) 245.
[10] J.A. Alonso, J. Sanz, J. Santamaría, C. León, A. Várez, M.T. Fernández-Díaz, Angew. Chem. Int. Ed. 39 (2000) 619.
[11] Y. Inaguma, M. Itoh, Solid State Ionics 86–88 (1996) 257.
[12] A. Rivera, C. León, J. Santamaría, A. Várez, O. V'yunov, A.G. Belous, J.A. Alonso, J. Sanz, Chem. Mater. 14 (2002) 5148.
[13] J. Rodríguez-Carvajal, Phys. B 192 (1992) 55.
[14] D. Massiot, WINFIT; Bruker-Franzen Analytik GmbH. Bremen, Germany, 1993.
[15] A.B. Boukamp, Solid State Ionics 20 (1986) 31.
[16] J.L. Fourquet, H. Duroy, M.P. Crosnier-López, J. Solid State Chem. 127 (1996) 283.
[17] M. Grüne, W. Müller-Warmutth, Ber. Bunsenges. Phys. Chem. 95 (1991) 1068.
[18] O. Kanert, R. Küchler, K.L. Ngai, H. Jain, Phys. Rev. B 49 (1994) 76.
[19] C. León, A. Rivera, A. Varez, J. Sanz, J. Santamaría, Phys. Rev. Lett. 86 (2001) 1279.
[20] D.P. Almond, G.K. Duncan, A.R. West, Solid State Ionics 9–10 (1983) 159.
[21] A.K. Jonscher, Dielectric Relaxation in Solids, Chelsea Dielectric Press, London, 1983.
[22] C. León, M.L. Lucía, J. Santamaría, M.A. París, J. Sanz, A. Várez, Phys. Rev. B 54 (1996) 184.
[23] L. Ngai, Comments Solid State Phys. 9 (1979) 127.
[24] K. Funke, Prog. Solid St. Chem. 22 (1993) 111.
[25] R. Winter, K. Siegmund, P. Heitjens, J. Non-Cryst. Solids 212 (1997) 215.
[26] C. León, J. Santamaría, M.A. París, J. Sanz, J. Ibarra, L.M. Torres, Phys. Rev. B 56 (1997) 5302.
[27] C. León, J. Santamaría, M.A. París, J. Sanz, J. Ibarra, A. Varez, J. Non-Cryst. Solids 235–237 (1998) 753.
[28] D.L. Sidebottom, Phys. Rev. B 83 (1999) 983.
[29] A.S. Nowick, B.S. Lim, Phys. Rev. B 63 (2001) 184115.
[30] R. Jiménez, A. Varez, J. Sanz, Solid State Ionics 179 (2008) 495.
[31] A.D. Robertson, A.R. West, A.G. Ritchie, Solid State Ionics 104 (1997) 1.
[32] J. Kincs, S.W. Martin, Phys. Rev. Lett. 76 (1996) 70.
[33] P. Maass, M. Meyer, A. Bunde, W. Dieterich, Phys. Rev. Lett. 77 (1996) 1528.
[34] J.P. Boilot, G. Collin, Ph. Colomban, R. Comes, Phys. Rev. B 22 (1980) 5912.
[35] J.L. Briant, G.C. Farrington, J. Solid State Chem. 33 (1980) 385.
[36] M.S. Whittingam, R.A. Huggins, J. Chem. Phys. 54 (1971) 414.
[37] J.-S. Lee, K.S. Yoo, T.S. Kim, H.J. Jung, Solid State Ionics 98 (1997) 15.
[38] O. Bohnke, C. Bohnke, J.L. Fourquet, Solid State Ionics 91 (1996) 21.
[39] R.D. Shannon, Acta Cryst. A32 (1976) 751.